PCCP

Accepted Manuscript

ROYAL SOCIETY OF CHEMISTRY

www.rsc.org/pccp

On the effects of substitution, intercalation, non-stoichiometry and block layer concept in TiS_2 based thermoelectrics

E. Guilmeau,[1*] A. Maignan,[1] C.Wan[2] and K. Koumoto[2]

[1] Laboratoire CRISMAT, UMR 6508 CNRS/ENSICAEN, 6 bd du Maréchal Juin

14050 CAEN Cedex 4, France.

[2] Department of Applied Chemistry, Graduate School of Engineering, Nagoya University,
Nagoya 464-8603, Japan

* E-mail: emmanuel.guilmeau@ensicaen.fr

Abstract

TiS_2 based layered sulfides have recently received increasing interest from the thermoelectric community. Due to its layered structure, TiS_2 compound with its enormous capacity for chemical substitution and intercalation offers different means to optimize the thermoelectric response through concomitant tuning of carrier concentration and decrease of the lattice thermal conductivity. In this review, we first discuss and summarize the crystal structures and physical/chemical properties of TiS_2 based layered sulfides. Then, the approaches that successfully enhanced the thermoelectric performances in the TiS_2 ceramic samples densified by Spark Plasma sintering are outlined, which include intercalation, non-stoichiometry, cationic substitution, and block layer concept.

A. Introduction

Over the last decade, the increase in global interest in research and development of thermoelectric (TE) materials has been partly due to the soaring short-term demand for energy and partly due to the need to find a sustainable future source of energy. Indeed, several sectors, such as automotive or industrial, could take advantage of thermoelectric materials capacity to directly convert the waste-heat into electrical energy, irrespective of source size and without the use of moving parts or the production of environmentally deleterious wastes. Moreover, thermoelectric generation systems offer the most viable method of exploiting the waste heat from automobiles, factories and similar sources. The efficiency and performance of thermoelectric energy conversion is related to the dimensionless figure of merit (ZT) of the thermoelectric materials, given by $ZT = S^2T/\kappa\rho$, where T is the absolute temperature, S is the Seebeck coefficient or thermoelectric power, ρ is the electrical resistivity, and κ is the total thermal conductivity.[1] To date, for low and medium temperature range applications (*i.e.* below 700 K), best performances are currently obtained by the well-known Bi_2Te_3 compound with maximum ZT values around 1 (or higher) at 400 K, or $AgPb_mSbTe_{2+m}$, Zn_4Sb_3, and $Yb_{0.19}Co_4Sb_{12}$ for temperatures between 400 K and 700 K.[2] However, it is well known that tellurium is toxic, scarce and expensive, preventing the use of Bi_2Te_3 for large scale applications. This has led to increasing efforts to find new environmentally-friendly, light and efficient thermoelectric materials in low and medium temperature ranges.

In the 2000's, Imai *et al.* have reported a large value of the Seebeck coefficient in TiS_2 (S = -250 µV/K at 300K) combined with a relatively low and metallic-like resistivity (ρ = 1.7 mΩ.cm at 300K).[3] In the following years, no great efforts have been devoted to this compound regarding thermoelectric applications and only recently, several studies have demonstrated its great potential as thermoelectric material.[4-8] In addition, TiS_2 offers several advantages for practical applications such as low toxicity, low cost and low density (3.25 g.cm^{-3}).

Unfortunately, the rather simple structure of TiS_2 composed of light elements is unfavorable for phonon scattering. Thermal conductivity is usually found above 4 W/mK at RT in pristine single crystals or bulk materials. One of the main strategies for developing TiS_2 compounds with enhanced ZT values is then to reduce κ whilst keeping high electrical performances. Due to its layered structure, TiS_2 compound offers the enormous capacity for chemical substitution and intercalation to provide a mechanism for optimizing the thermoelectric response through tuning of the transport properties and in the same time decreasing the lattice thermal conductivity. The Seebeck coefficient and the electrical conductivity of the TiS_2 layered compounds can then be optimized through change in charge carrier concentration, so the power factor can be potentially increased in a specified temperature range. Also the intercalated layer or substituted element in the structure can potentially create disorder and phonon scattering reducing the lattice thermal conductivity. The overall ZT value of the material can be then potentially increased using intercalation and substitution approaches.

Structurally, TiS_2 also offers the possibility to intercalate full block layers between the CdI_2 layers forming the so-called misfit compounds. These natural superlattices with general formula $(MX)_{1+x}(TX_2)_n$, (M = Pb, Bi, Sn, Sb, rare-earth elements; T = Ti, V, Cr, Nb, Ta; X = S, Se; n = 1, 2, 3) are built by intercalating a MS layer into the van der Waals gap of layered TiS_2.[9] The intercalated block layer was proved to suppress phonon transport, which is attributed to softening of the transverse sound velocities due to weakened interlayer bonding. The thermoelectric properties are then enhanced making these natural superlattice structures as possible candidate high-performance thermoelectric materials.

Based on the above cited approaches, we show in this review how the thermoelectric properties can be modified in crystallographic structures based on TiS_2 type layer, by playing with 1) intercalation, 2) substitution, 3) non-stoichiometry and 4) block layer concept. From these different studies, TiS_2 appears as a model structure for the study of the mechanisms, which govern the electrical and thermal transport properties of materials for thermoelectric applications.

B. Crystal structure and electrical properties

TiS_2 belongs to the layered transition metal dichalcogenides (TMDC's) MX_2 (M is a transition metal atom from the group IVb, Vb or VIb columns of the periodic table, X = S, Se, or Te) which have been attractive compounds over a long term of years due to the rich variety of the physical properties.[10-12] Depending on the structure type and constituting elements, the TMDC compounds can exhibit either insulating (HfS_2), semiconductor (ZrS_2), or metal like behavior (NbS_2, TaS_2). The question, of whether TiS_2 is intrinsically semiconducting or semimetallic, has been intensively investigated for more than four decades. It has presented a challenge study to both experimental and theoretical techniques which is still under debate.[13-21] It is nevertheless well accepted that the main explanation of discrepancies in terms of physical properties originates from non-stoichiometry in the so-called $Ti_{1+x}S_2$. The effect of non-stoichiometry on the thermoelectric properties will be presented in paragraph D.2.

In its most common form (1*T*), bulk titanium disulphide (TiS_2) crystallizes in a hexagonal layered structure ($P\bar{3}m$-1) consisting of one hexagonally packed sheet of metal atoms contained between two hexagonal sheets of chalcogens for each layer, where atoms within a layer are bound by strong covalent forces. This structural arrangement leads to metal atoms surrounded by six chalcogen atoms in an octahedral environment (Fig. 1a), resulting in weak chalcogen-chalcogen van der Waals interactions between adjacent layers with S-Ti-S slabs stacked along the *c* axis. ($c = 5.6912$ Å)

As shown in Figure 2, the crystal structure of misfit $(MS)_{1+x}(TiS_2)_2$ compounds is composed of a *M*S layer sandwiched by paired TiS_2 layers separated by a van der Waals gap.[9] The atomic structure of a $(PbS)_{1.18}(TiS_2)_2$ single crystal has been previously refined.[22] The Pb and S(1) atoms of the PbS subsystem are on the 4(*i*) sites of space group C2/m; each Pb atom is coordinated by five S atoms located at the corners of a slightly distorted square pyramid (NaCl structure). As Pb atoms protrude from the sulfur planes on both sides, each Pb atom is also bonded to the S atoms of the TiS_2 slabs by weak covalent force. The atoms of the $(TiS_2)_2$ subsystem are on 2(*e*) sites of space group $C2_1/m$. Each Ti atom is coordinated by six S atoms in a trigonal antiprismatic arrangement. The TiS_2 slab is slightly distorted compared with 1*T*-TiS_2, in which Ti is octahedrally coordinated.

C. Experimental details

All of the TiS_2 series were synthesized in a two steps process including sealed tube synthesis and Spark Plasma Sintering. For the Cu_xTiS_2 series, TiS_2 powder was first synthesized in sealed silica tube at 923K/12h from the stoichiometric mixture of pure elements. Then, this powder was ground and mixed with Cu in stoichiometric amounts (Details in Ref. [5]). For the Ag_xTiS_2 series, silver, titanium and sulfur were mixed together and synthesized in sealed silica tube at 923K/12h (Details in Ref. [23]). For the $Ti_{1-x}Ta_xS_2$ series, the powders were synthesized by two successive heating steps in sealed fused silica tubes.[24] The powders were first heated at 1223K, then grinded, pelletized and heated again at 1273K for 48h. For the $Ti_{1-x}Nb_xS_2$ series, pure elements were mixed and synthesized in sealed silica tubes at 905K for 12h.[25] The non-stoichiometric $Ti_{1+x}S_2$ series was synthesized in sealed silica tubes at 905K for 12h. All the as-synthesized powders were agglomerated and composed of plate-like grains of

1-10 µm (in the *ab* plane) depending of the heating temperature. The powders were ground and sieved down to 200 µm.

Cu_xTiS_2, Ag_xTiS_2, and $Ti_{1-x}Ta_xS_2$ powders were placed in graphite dies of 15 mm diameter and densified by Spark Plasma Sintering (SPS) (FCT HPD 25) at 1073-1173K for 10-30 min under a pressure of 50 MPa. $Ti_{1-x}Nb_xS_2$ and $Ti_{1+x}S_2$ powders were placed in tungsten carbide (WC) dies of 10 mm diameter and densified by the same SPS machine at 873K for 30 min under a pressure of 300 MPa. The use of WC dies at low sintering temperature (873K) prevents from sulfur volatilization; this will be discussed latter.

After SPS, the final dimensions of the pellets are around 7 mm in thickness and 10-15 mm in diameter. The geometrical densities range between 95% and 100% of the theoretical ones.

The $(MS)_{1+x}(TiS_2)_2$ (M = Bi, Sn, Pb) powders were prepared using a solid-liquid-vapor reaction method. For each composition, the M, S, Ti powders were mixed in the molar ratio of 1:2:5 and then sealed in an evacuated silica tube. The silica tube was then fired in an electric furnace at 773K for 12 h, then at 1073K for 48 h and finally cooled down to room temperature. The obtained powders with luster were ground and sieved. SPS method (SPS-1050, Sumitomo Mining Coal Mining Co. Ltd.) was also used to densify the powders at 973K for 10 min under the pressure of 50 MPa into a pellet with diameter of 15 mm and thickness of 6 mm.

Since the microstructures of all the samples in the present review are anisotropic, these latter were deliberately machined for thermoelectric properties measurements in the direction perpendicular to the pressure.

Thermoelectric property measurements have been performed on samples extracted from the same pellet. For section D.1, D.2 and D.3, Seebeck coefficient and electrical resistivity were measured from RT to 700K on an Ulvac Riko ZEM3 system under partial pressure of helium. Similarly, a Netzsch 457 microflash laser flash system was used to assess the thermal diffusivity under dynamic N_2 flow. Thermal conductivity was calculated from the product of thermal diffusivity, density and heat capacity. The latter was measured using a commercial Netzsch DSC STA 449 F3 Jupiter. The values were found to be very close to those obtained by using the Dulong-Petit approximation (0.42 $J.g^{-1}.K^{-1}$). Hall-effect experiments were carried out at 300K using a Physical Properties Measurement System (PPMS Quantum Design) in a magnetic field up to 7 T. For section D.4, the Seebeck coefficient and electrical conductivity were measured simultaneously by a conventional steady-state method and a four-probe method, respectively, in an Ar atmosphere at 300 K to 773 K (RZ-2001K;Ozawa Science). The carrier concentration was determined by Hall-effect measurements with a van der Pauw electrode configuration under a vacuum of 10^{-3} Pa over the same temperature range (Resi Test 8300; Toyo Technica). The heat capacity and thermal diffusivity were measured by differential scanning calorimetry (DSC-2910; TA Instruments) and a laser-flash method (TC-9000V; ULVAC-RIKO), respectively. The thermal conductivity was calculated as the product of density, heat capacity, and thermal diffusivity.

From these measurements, the average zT uncertainty is about 15-20%.

Details on the structural characterizations are given in the respective cited references.

D. Results and Discussion

D. 1. Intercalation and staging effect in Ag_xTiS_2 and Cu_xTiS_2

TiS_2 is one of the most well-known intercalation compounds. Its van der Waals gap can be filled by various types of chemical moieties such as molecules,[26] structural blocks made of a stacking of several atomic layers in the case of “misfit” TiS_2 phases,[4,27,28] or metallic atoms such as the 3*d* Ti metal (self-intercalation according to $Ti_{1+x}S_2$, see the non-stoichiometry section), Mn, Fe, Co, Ni, Cu and heavier metals such as Ag and Bi or alkaline cations (Na, Li).[29-36] The intercalants act on both crystallographic and electronic structures. On the one hand, depending on the size of the intercalants and the degree of its covalency to the neighboring S layers, the distance between two successive TiS_2 layers can be increased or decreased. For instance, the *c* unit-cell parameter decreases as Co is intercalated in TiS_2 from 5.70 Å for stoichiometric TiS_2 down to 5.62 Å for $Co_{0.57}TiS_2$,[37,38] whereas *c* increases rapidly with Cu, to reach 5.76 Å for $Cu_{0.1}TiS_2$.[5] The *c* contraction in the case of Co is explained by the very covalent character of the Co-S bonding.[37] On the other hand, depending on the electronic transfer between the intercalates and the TiS_2 layer, more or less charges are transferred in the empty 3*d* orbitals of titanium, indicating that through these species, the doping level of the “TiS_2” can be tuned.

Interestingly, intercalations can induce also complex in-plane superstructures, as for Co or Ag with ordering of the metal cations occupation into the crystallographic sites of the van der Waals gap: in the case of Ag_xTiS_2, the $a\sqrt{3} \times a\sqrt{3}$ superlattice has been evidenced for temperatures just below room temperature.[39] In addition, silver is a peculiar intercalant as it favors staging, *i.e.* out-of-plane ordering phenomena. In the following, a comparison between

Cu_xTiS_2 and Ag_xTiS_2 is made to illustrate the different effect of these intercalations on the crystallographic structure and a comparison of their thermoelectric properties is also given.

Copper intercalation leads to the so-called stage 1 structure of M_xTiS_2, where M is a metal, at least for small amounts ($x \leq 0.1$ in ref. [5]). In that case, as for all 3d M intercalants, a continuous x variable content of M cations is randomly distributed into the successive van der Waals gaps (Fig. 1b). Accordingly, the c unit-cell parameter for Cu_xTiS_2 increases monotonously from 5.707(1) Å to 5.759(1) Å as x increases from x=0 to x=0.1 (Fig. 3). The veracity of the intercalation is also confirmed by EDS analysis coupled to electron diffraction within a transmission electron microscope.

This monotonous evolution is in marked contrast with the situation encountered in the Ag_xTiS_2 case, a series for which dense ceramics can be also obtained by SPS.[23] In fact, for x = 0.2, a large fraction of the sample (about 85%) crystallizes in the so-called stage 2 form (Fig. 1c): this structure, ideally written $Ag_{1/6}TiS_2$, consists in the 1:1 stacking of empty or one third filled van der Waals gaps. The crystallographic space group is $P\bar{3}m$-1 with a = 3.416(4) Å and c = 12.100(2) Å. The structural refinement of the "$Ag_{0.2}TiS_2$" nominal composition leads to a 85%-15% mixture of stage 2, with a = 3.416(1) Å and c = 12.110(1) Å, *i.e.* values very close to those just mentioned for $Ag_{1/6}TiS_2$, coexisting with a stage 1 Ag_xTiS_2 phase. The latter corresponds to random distribution of Ag over the crystallographic sites in every successive van der Waals gaps (Fig. 1b) as in the case of Cu_xTiS_2. Nevertheless, in this stage 1 phase, the c cell-unit parameter (6.053(1) Å) is much larger than in the case of Cu_xTiS_2 (x=0.1, Table1). It is clear that this stage 1 phase corresponds to a Ag rich phase, consistently with the nominal content beyond the ideal x=1/6 value of the stage 2. Thus, this Ag_xTiS_2 ceramic series can be described as composites. In fact they are all made of a mixture of stage 1 and stage 2 phases. Even by starting from "$Ag_{0.05}TiS_2$", a phase mixture of a majority (95%) of stage 1, with a = 3.408(1) Å and c = 5.710(1) Å, and a stage 2 phase (5%), with a = 3.409(1) Å, and c = 11.570(2) Å, is obtained. For the Ag_xTiS_2, the c unit-cell parameter increases with x (Fig. 3), confirming the Ag content intercalated between the layers increases in both stage 1 and stage 2 phases. When compared to Cu_xTiS_2, the c unit-cell parameter values for the stage 1 are significantly lower with c=5.759 Å and c=5.717(2) Å for $Cu_{0.1}TiS_2$ and $Ag_{0.1}TiS_2$, respectively. This is in fair agreement with the formation of Ag rich stage 2 phase in Ag_xTiS_2.

The presence of a majority of either stage 2 or stage 1 phase in "$Ag_{0.2}TiS_2$" and "$Ag_{0.05}TiS_2$", is confirmed by the [010] electron diffraction patterns (Fig. 4b) which show the presence of additional spots along the [001] direction for the former corresponding to the *c* doubling. Accordingly, the presence of the two different phases in Ag_xTiS_2 induces an important local atomic disorder as illustrated by the high resolution TEM image of "$Ag_{0.1}TiS_2$" with the presence of local regions of stage 2 in the stage 1 matrix (Fig. 4c). The presence of streaks on the main spots in the [010] electron diffraction pattern (Inset Fig. 4c) indicates the presence of stacking faults. The elongations of the (00*l*) spots are consistent with local variations of the *c* axis values as a result of the closeness of the *c* parameter for the stage 1 and *c*/2 for the stage 2 phase. It supports that the distance between two successive layers is spontaneously increased or decreased, which confirms that the silver cations are randomly distributed in the TiS_2 host structure. In $Ag_{0.05}TiS_2$ (Fig 4a), the absence of diffuse line along the [001] direction indicates the structure is less disordered as compared to the silver rich samples.

Although, the structural features of Cu_xTiS_2 and Ag_xTiS_2 differ, it is remarkable that their physical properties (ρ, S) are very similar (Fig. 5). At 700K and for x=0.10 in M_xTiS_2, the electrical resistivity and Seebeck coefficient are equal to 1.4 mΩ.cm and -125 µV/K for Cu, and 2.1 mΩ.cm and -154 µV/K for Ag. This leads to very similar *PF* values, PF_{700K}=1.09 mW/mK^2 and PF_{700K}=1.12 mW/mK^2 for $Cu_{0.1}TiS_2$ and $Ag_{0.1}TiS_2$, respectively (Table 1). These results support the fact that both types of intercalating cations provide charges to the neighboring TiS_2 slabs which is confirmed by the Hall measurements at 300K performed to estimate the electron concentration, with $n = 3.7x10^{21}cm^{-3}$ for $Cu_{0.1}TiS_2$ to be compared to $n = 0.65x10^{21}cm^{-3}$ in the "TiS_2" ceramic prepared by using the same SPS conditions (Table 1).

For both Ag and Cu, it is found that these cations are very efficient to increase the phonon scattering through structural disorder, described above. The thermal conductivity (κ), and the lattice part (κ_L) deduced by subtracting the electronic part (κ_e) to κ, are given in Fig. 6. For $Ag_{0.1}TiS_2$ and $Cu_{0.1}TiS_2$, κ values at 700K are close to 1.8 to 2 W/mK. It must be emphasized that such κ values are very similar to those reported for TiS_2 prepared with the same process, *i.e.* κ~2.0-2.1 W/mK. Taking into account the ρ decrease as x increases in M_xTiS_2 with M=Ag or Cu, this demonstrates that these intercalations are very efficient to reduce the lattice part of the thermal conductivity (κ_L). At 700K, κ_L decreases from ~1.8 W/mK in TiS_2 down to 0.8-0.9 W/mK in $M_{0.1}TiS_2$ (M=Ag or Cu). Accordingly, the *ZT* values are relatively close at 700K with *ZT*=0.46 for $Ag_{0.1}TiS_2$ against *ZT*=0.38 for $Cu_{0.1}TiS_2$ (Table 1).

D.2. Role of non-Stoichiometry

The TiS_2 layered structure offers as well a great flexibility, with large non stoichiometry range (*i.e.* $Ti_{1+x}S_2$). TiS_2 is a Pauli paramagnet, but its electronic structure has been debated for several decades to determine if TiS_2 is a semimetal or semiconductor. This debate is directly linked to the TiS_2 stoichiometry, in which defects and doping are difficult to control. The existence of stoichiometric TiS_2 is still controversial. In fact, it is well known and accepted that TiS_2 tends to grow metal rich and that the excess Ti atoms intercalate into the Van der Waals gap, leading to $Ti_{1+x}S_2$. Each excess Ti atom is assumed to be donor of four electrons to the conduction band. This off-stoichiometry is the main explanation of discrepancies in terms of physical and thermoelectric properties of the so-called TiS_2. Despite its rather simple composition, the synthesis of stoichiometric TiS_2 is complex. Atmosphere, pressure, temperature and synthesis conditions are among many factors which can affect sulfur volatilization. For example, Jeannin *et al.* firstly reported it was not possible to synthesize stoichiometric TiS_2.[40,41] Later, Mikkelsen *et al.*[42] reported that the ideal temperature for stabilizing stoichiometric TiS_2 is 632ºC. Above this temperature, the off-stoichiometry is inherent due to the sulfur loss.

In the view point of thermoelectric properties, a wide range of Seebeck coefficient, electrical resistivity, and thermal conductivity values can be found for the so-called TiS_2.[3,4,18,21,24,25,43-47] Thermoelectric properties are greatly dependent on the off-stoichiometry, which controls the charge carrier concentration. As a result, a spread range of Seebeck coefficient values can be found in $1T$-$Ti_{1+x}S_2$. For example, Thompson *et al.*[17] reported the highest Seebeck coefficient for TiS_2 around -270μV/K whereas this coefficient is divided by around five (-60μV/K) in $Ti_{1.05}S_2$.

It appeared then of fundamental importance to understand the influence of Ti/S stoichiometry on the thermoelectric properties of TiS_2. If optimization of the power factor is possible by controlling the off-stoichiometry, *i.e.* the carrier concentration, the above results obtained on Ag_xTiS_2 and Cu_xTiS_2 suggest that the thermal conductivity could be reduced in the same time through structural disorder induced by the self-intercalation of Ti atoms in TiS_2 layers, even in a small amount. Based on this concept, we have investigated in details the effect of non-stoichiometry on the electrical and thermal properties in the $Ti_{1+x}S_2$ series.[6]

From a structural point of view, XRD patterns confirm that, for all x values in the range $0 \leq x \leq 0.05$, a single phase derived from TiS_2 is obtained. All XRD patterns were well described in the trigonal space group $P\bar{3}m1$ of the TiS_2 host structure. Intercalation results in a systematic expansion of the unit-cell axis along the stacking direction and of the unit-cell volume. The c parameter increases from 5.678(1) Å for $x = 0$ to 5.715(1) Å for x=0.05 (Table 1).

The temperature dependence of the electrical resistivity in the $Ti_{1+x}S_2$ series is displayed in Figure 7. The electrical resistivity curves demonstrate a general tendency towards more conducting behavior as the Ti interstitial atom content increases. We note that the electrical resistivity of the heavily doped compound $Ti_{1.05}S_2$ is almost independent with temperature. The present results show some similarities with the behavior of alkali or metal intercalated TiS_2, where a charge-transfer mechanism is classically used to account for the observed phenomena. As discussed above, it is reasonable to assume here that the valence electrons of the intercalated metallic titanium atoms transfer to the Ti 3*d* band of the host, leading to an increase of electron concentration (Table 1) and enhancement of the metallic behavior of $Ti_{1+x}S_2$. This suggestion is also consistent with the decreased Seebeck coefficient (300K) when increasing x content (Figure 8). If we compare our data with previous studies, our results are closest to those reported by Thompson *et al.* in 1975.[17] As we can observe from Fig. 8, a wide range of Seebeck coefficient values ranging from -38 µV/K for Li *et al.*[46] to -270 µV/K for Thompson *et al.* have been reported for the so-called TiS_2, whilst intermediate values of *ca*. -160 µV/K and -80 µV/K were obtained by Guilmeau *et al.*[5] and Wan *et al.*[4] respectively. Of course, the main explanation of such a large variation in Seebeck coefficient values comes from differences in sample preparation that leads to different Ti/S ratios due to sulphur loss.

It must be also pointed out that the magnitudes of the Seebeck coefficient and electrical resistivity are rather comparable between the three first members of our series (*i.e.* x=0, x=0.005 and x=0.01). This repeatable behavior is mainly explained by the slight oxidation of TiS_2 into TiO_2 which occurs during SPS treatment. If TiO_{2-y} traces have not been systematically detected in the XRD patterns of our samples (usually in the detection limit), the oxidation most probably originates from hydroxide or H_2O adsorption on the powder after sealed tube synthesis. As a consequence, the Ti content between the layers decreases due to the oxidation reaction during SPS and induces a decrease in carrier concentration, corresponding to an increase in Seebeck coefficient and electrical resistivity. Therefore, the slight increase in carrier concentration induced by off-stoichiometry is balanced by the titanium de-intercalation during SPS (decrease in carrier concentration). The first three members of the series have then quite similar properties when measured after SPS. It is also interesting to note that the absolute value of the Seebeck coefficient measured before SPS (on pressed powders) is lower as compared to SPS samples, which supports the idea that few Ti cations de-intercalate during oxidation reaction in SPS. Such behaviour was never observed before and confirms the high sensibility of TiS_2 to oxidation. Finally, the saturation of $|S|$ close to 300 μV/K in powder or bulk specimens also indicates that the stoichiometric composition is certainly achieved (or very close). To our knowledge, such value was never reported on TiS_2 before.

As for other intercalated TiS_2 compounds like Ag_xTiS_2, Cu_xTiS_2 and Nd_xTiS_2,[45] the presence of titanium in the intercalation sites decreases the lattice part of the thermal conductivity. The Ti intercalation between the TiS_2 layers generates disorder and phonon scattering even for a small excess of titanium. As shown in Figure 9, the lattice and total thermal conductivity respectively decrease with Ti off-stoichiometry. As reported recently by Wan *et al.*[4] in $(MS)_{1+x}(TiS_2)_2$ (M=Pb, Bi, Sn) misfit layer compounds, the decrease in the lattice thermal conductivity may be linked to the weak interlayer bonding and disruption of periodicity of the TiS_2 layers in the direction perpendicular to the layers by the intercalated Ti layers. HRTEM study of the $Ti_{1.05}S_2$ sample (Figure 10) supports the existence of local disordering forming a “wavy” structure related to local intercalation of Ti between successive TiS_2 slabs. The magnitude of the κ_L reduction (54% in the present study from $x = 0$ to $x = 0.025$ at 300 K) through Ti intercalation is in good agreement with intercalated Cu_xTiS_2, Nd_xTiS_2 and misfit $(SnS)_{1.2}(TiS_2)_2$ compounds which exhibit a substantial decrease of between 30% and 50%.[4,5,45] The decrease with x appears more important in this series as compared to Ag_xTiS_2 and Cu_xTiS_2 (Figure 6). This is mainly explained by the more stoichiometric nature of the pristine x=0 compound in the $Ti_{1+x}S_2$ series. This result suggests that the creation of an intermediate layer even composed of few intercalated metal cations is a highly efficient approach to decrease the thermal conductivity of TiS_2. In summary, controlled Ti/S stoichiometry allowed optimization of the electrical properties with optimum power factors of ~1.7 mW/mK^2 at 300 K and 1.04 mW/mK^2 at 700 K achieved for $x = 0.015$ and $x = 0.02$, respectively. The thermal conductivity being drastically reduced by effective phonon scattering through Ti intercalation in off-stoichiometric compounds, the resulting ZT is enhanced up to 0.48 at 700 K for x=0.025.

D.3. Solid solutions $Ti_{1-x}Ta_xS_2$, $Ti_{1-x}Nb_xS_2$

First proposed by Ioffe in 1956,[48] the formation of solid solution from isotructural compounds (alloying effect) is a time-honored technique of reducing lattice thermal conductivity that has been used in the development of all state of the art thermoelectric materials.[49] Solid solutions are archetypes examples of point defects scattering where both mass and strain fluctuations tend to effectively scatter high frequency phonons. Mass fluctuations scattering is probably the easier chemical way to deal with, and in fact, might be the major contribution in many semiconductor solid solutions. A particular solid solution will be benefit to thermoelectricity (improvement in ZT) provided the ratio of its mobility to its lattice thermal conductivity is larger than for pristine compounds constituting solid solution.

From the literature, few papers have been devoted to the study of solid solutions in TiS_2. Most of them concerns $Ti_{1-x}Ta_xS_2$,[50-53] $Ti_{1-x}Nb_xS_2$,[54] $Ti_{1-x}Cr_xS_2$,[55-56] $Ti_{1-x}V_xS_2$,[57] $Ti_{1-x}Zr_xS_2$.[58] From fundamental aspects, this type of substitution offers various possibilities for the manipulation of the d electron concentration and the examination of the effects of that concentration on the electrical, magnetic, and thermal properties of the system. In fact, for thermoelectric properties, such chemical approach offers the possibility to tune the carrier concentration of TiS_2, while, in the same time, to scatter phonons through structural disorder, point defects and/or mass fluctuations effects. Also, if electrical properties of the above solid solutions have been solely studied at low temperature, it is wise to determine both the electrical and thermal properties at higher temperatures. We have deemed appropriate to revisit the synthesis of $Ti_{1-x}Ta_xS_2$ and $Ti_{1-x}Nb_xS_2$ series and to examine their thermoelectric properties.

TiS_2 and TaS_2 are known to exhibit different crystal symmetries related to the layered MX_2 dichalcogenide structure type. While TiS_2 crystallizes mainly in the 1T form, TaS_2 can adopt several forms, referred as 1T, 2H, 3R, 4H, 6R phases, and NbS_2 only 2H and 3R forms. For 1T-TiS_2, CdI_2 layer is composed of edge-shared octahedra of TiS_6 that form infinite layers perpendicular to the c axis. Differently, in 3R-TaS_2 and 3R-NbS_2, metal atoms are in trigonal prismatic coordination typical from some MX_2 phases.

All the structure of the series $Ti_{1-x}Ta_xS_2$ (for $x \leq 0.4$) were well refined in the aristotype space group $P\bar{3}m1$, which implies a statistic distribution of the titanium and tantalum atoms over the same crystallographic site (Ti/Ta 1a: 0, 0, 0 and S 2d : 1/3, 2/3, z). Above $x = 0.4$, the XRD pattern can be refined as a mixture of 1T-TiS_2 and 3R-TaS_2 phases. This result differs from previous studies where the substitution replacement of Ta for Ti seems to stabilize the octahedral 1T phase on the full range of the solid solution ($0 \leq x \leq 1$). Shorten annealing dwell time in our study is probably the main explanation to such difference. Nevertheless, 3R-TaS_2

showing a metallic-like behavior with low Seebeck coefficient,[10,11] our study remained focused on only the single phases with $x \leq 0.4$. The existence of this $Ti_{1-x}Ta_xS_2$ solid solution (for $x \leq 0.4$) was confirmed by the linear evolution of cell parameters that follows Vegard's law with x varying from 0 to 0.4 (Table 1).[24] Indeed, between the two end members from $x = 0$ to $x = 0.4$, the average spacing between TiS_2 layers (c parameter) expands linearly from 5.704(1) Å to 5.781(1) Å as Ta content increases; correspondingly, the a parameter decreases slightly from 3.407(1) Å to 3.388(1) Å. These results confirm the MS_6 octahedron distortion along the 3-fold axis due to the different ionic radius (0.605 Å for Ti^{4+} and 0.68 Å for Ta^{4+}), as suggested in $Ti_{1-x}Ta_xS_2$ solid solution.[53] Such behaviour of lattice parameters a and c is also found in our $Ti_{1-x}Nb_xS_2$ series ($0 \leq x \leq 0.05$),[25] as also previously observed in $Ti_{1-x}Nb_xS_2$ series ($0 \leq x \leq 1$)[54] and $W_{1-x}Mo_xS_2$ ($0 \leq x \leq 1$) solid solution.[59] The evolution of the cell parameters is given in table 1. In the $Ti_{1-x}Nb_xS_2$ series, to prevent from any sulfur loss during synthesis, single phase with 1T crystallographic form was obtained at lower temperature (905K). The solid solution then exists only for $x \leq 0.05$, the 3R-NbS_2 phase being present above this value. On the other hand, the decrease in a parameter indicates that Ta/Nb for Ti substitution takes place in the structure and that intercalation between TiS_2 slabs unlikely occurs. This assumption is confirmed by HRTEM observations in which no structural defects or "wavy" layers are observed (Figure 11).

The temperature dependence of the electrical resistivity in the $Ti_{1-x}Ta_xS_2$ and $Ti_{1-x}Nb_xS_2$ series is displayed in Figure 12a. A difference of one order of magnitude is observed between the two series which is due to the drastic sulphur volatilization occurring during the process at high temperature requested for the formation of the $Ti_{1-x}Ta_xS_2$ solid solution (*i.e.* 1223-1273K, see experimental part, against 905-923K in the other series). In addition, $Ti_{1-x}Nb_xS_2$ compounds were densified using WC dies at 873K (like in $Ti_{1+x}S_2$ series), which also helps in preventing from sulfur loss. As mentioned above, sulfur volatilization generates excess titanium atoms which intercalates into the van der Waals gap. This generates conduction electrons in the Ti *3d* band by charge transfer, and increases the carrier concentration (table 1), as confirmed by the low Seebeck values measured in the $Ti_{1-x}Ta_xS_2$ series (Figure 12b). The c cell parameters for x=0 and x=0.05 are also found higher in $Ti_{1-x}Ta_xS_2$ than in $Ti_{1-x}Nb_xS_2$, which is in good agreement with significant Ti self-intercalation in $Ti_{1-x}Ta_xS_2$

As an overall trend for both series, the electrical resistivity and Seebeck coefficient curves demonstrate a clear tendency towards more conducting behavior as the Ta/Nb content increases. This more metallic behavior is also confirmed by the decreasing magnitude of the slope of the electrical resistivity as a function of temperature when Ta content increases. Such behavior is explained by the increase of the overlap between the atomic orbitals of the metal, when the titanium atoms are gradually replaced by tantalum or niobium ones. As a consequence, the binding character of the metal/metal interaction increases in the $Ti_{1-x}(Ta,Nb)_xS_2$ series when x content increases. In addition, Y. Tison *et al.*[53] have clearly shown that energetic dispersion of the t_{2g} levels is higher for TaS_2 (4.1 eV) than for TiS_2 (2.1 eV), in agreement with the literature. This band dispersion can directly be correlated to the binding metal-metal interactions which takes part in a non-negligible way in cohesion of tantalum disulphide while such metallic bonds are less considered in titanium disulphide. Such effect is also valid in $Ti_{1-x}Nb_xS_2$ series. Finally, because of the different electronic configuration of the metal atoms in their sulfur environment ($Ti^{4+}(d^0)$, Ta^{4+},$Nb^{4+}(d^1)$), the conduction band is empty for TiS_2 and partially filled when Ta/Nb for Ti substitution takes place, increasing the carrier concentration in each series. Furthermore, as expected, the Hall mobility decreases with Ta/Nb content as seen in Table 1. This is in good agreement with previous papers[50,51] and confirms increased scattering effect due to an increase in charge carrier concentration. The power factor does not exceed 0.7 mW/mK^2 in both series (Table 1), and is significantly lower than in Cu_xTiS_2, Ag_xTiS_2, and $Ti_{1+x}S_2$ series. Since the optimum carrier concentration in TiS_2 was determined between 0.5 and 3×10^{21} cm^{-3} (bold numbers in table 1), these low *PF* values are mainly related to the carrier concentration which is too low in Nb-substituted compounds ($n < 0.5\times10^{21}$ cm^{-3}) and too high in Ta-substituted series ($n > 3\times10^{21}$ cm^{-3}). In addition, the increased electron scattering in substituted compounds (higher x content) generates lower mobilities. It highlights the crucial role of non-stoichiometry in TiS_2, and the importance of process conditions to control the Ti/S ratio in the final product and to optimize the electrical properties.

The temperature dependences of the total thermal conductivity κ and lattice contribution κ_L for $Ti_{1-x}Ta_xS_2$ and $Ti_{1-x}Nb_xS_2$ series are respectively displayed in Figure 13 and 14. It can be seen that, in both series, κ does not significantly increase with x content whereas the electronic contribution increases significantly with x due to charge carriers doping. In addition, it is obvious that the total and lattice thermal conductivity are significantly larger in the $Ti_{1-x}Nb_xS_2$ series than in the $Ti_{1-x}Ta_xS_2$ one. Such difference is mainly explained by two effects: 1) Ta-substituted compounds are self-intercalated by Ti cations which induces phonon scattering due to structural disorder (See paragraph on non-stoichiometry), 2) the relative densities are higher in $Ti_{1-x}Nb_xS_2$ series (close to 100%) than in the $Ti_{1-x}Ta_xS_2$ (>95%), due to higher SPS pressure (300 MPa against 50 MPa).

Regarding the evolution of the lattice thermal conductvity with x, it can be seen that κ_L decreases significantly with Ta/Nb content. As expected, the partial substitution of heavy elements (tantalum, niobium) for constituent elements (titanium) reduces the lattice thermal conductivity. The origin of this behaviour may be due to two principal effects, namely structural disorder/deformation due to octahedral distortion and/or mass fluctuation effect. For a quantitative and better understanding of this change in lattice thermal conductivity in this system, we have analyzed its temperature dependence by Debye-Callaway model.[60] The strain effect was analyzed based on the observed lattice volume change with Ta/Nb amount, and was found to be negligible compared with mass effect. Structural disorder/deformation from octahedral distorsion, as discussed before, in the layers due to the higher tantalum radius compared to titanium radius may be then excluded as a major contribution for the decrease in the lattice thermal conductivity. The mass difference between Ti and Ta/Nb then effectively depresses the κ_L in this system.

As shown in Table 1, the ZT is enhanced by Ta/Nb substitution in TiS_2 below x=0.05. Since the carrier concentration and power factor are not optimized, the figure of merit ZT remains lower than in the other studied systems. Control of Ti/S ratio in the final product is then required to enhance the thermoelectric properties. Other substitution (Zr, Cr, V) may be an alternative approach to control the carrier concentration in TiS_2 based solid solutions for better thermoelectric performances.

D.4. Block layer concept

In order to maintain the high power factor of the layered TiS_2 while reducing the thermal conductivity, we propose a natural superlattice structure by intercalating one layer of MS (M=Pb, Sn, Bi) into the van der Waals gap of TiS_2, forming misfit layer compounds $(MS)_{1+x}(TiS_2)_2$. The electron path inside the TiS_2 layers would not be destroyed and the intercalated MS layer could behave as a phonon-blocking layer which can significantly reduce the thermal conductivity.[4,27,28]

In the "in-plane" direction, the electrical conductivities of all $(MS)_{1+x}(TiS_2)_2$ compounds are higher than that of TiS_2 and the Hall measurement confirms the higher carrier concentrations in the former compounds (Fig. 15). It has been realized there electron transfer from the MX layer to the TiS_2 layers and additional covalent bonding between the M atoms and the sulfur atoms in the MX layer are formed.[9] From the carrier concentrations and the lattice parameters, we can estimate the number of electrons received per Ti atom for $(BiS)_{1.2}(TiS_2)_2$, $(SnS)_{1.2}(TiS_2)_2$ and $(PbS)_{1.18}(TiS_2)_2$ is 0.45, 0.16 and 0.2, respectively. Much more electron transfer takes place in $(BiS)_{1.2}(TiS_2)_2$ than the other two compositions, because the nominal valence of bismuth is 3+ here and the BiS layer could have one more electron transferred to the TiS_2 layers. Despite the increase of carrier concentration, the mobility of the misfit layer compound is almost maintained compared with that of TiS_2, as the electron transport path inside the TiS_2 layers is not destroyed. The Seebeck coefficients of $(M\mathrm{S})_{1+x}(TiS_2)_2$ are decreased compared with that of TiS_2. In $(M\mathrm{S})_{1+\mathrm{x}}(TiS_2)_2$, a rigid band model can hold and the band structure is a superposition of those of *M*S and TiS_2 subsystem. The *d* orbitals of Ti play a dominant role in determining the transport properties. Therefore, the electron transfer from the *M*S layer could increase the degree of band filling and consequent upward shift of the Fermi level in the 3*d* orbital. As a result, the Seebeck coefficients of all the misfit layer compounds were all lower than that of TiS_2.

All the $(M\mathrm{S})_{1+\mathrm{x}}(TiS_2)_2$ compositions have lower thermal conductivities than TiS_2 in the in-plane direction in the whole temperature range. The thermal conductivity is contributed by both phonons and electrons, where the electronic thermal conductivity could be estimated by the Wiedemann-Franz law. Compared with pure TiS_2, the misfit compounds also have much lower lattice thermal conductivities, which is related with their complex layered structure. As indicated by the kinetic theory, $k=1/3C_\mathrm{v}Vl$, where C_v, V and l represent the heat capacity, sound velocity, and phonon mean free path respectively. The sound velocity has three polarization modes, including one longitudinal mode and two transverse modes. In the in-plane direction, the two transverse velocities are not equal because of the layered structure. Compared with pure TiS_2, the longitudinal velocities of the misfit layer compounds are slightly decreased, which can be attributed to the density increase. In contrast, the transverse sound velocities, especially V_T1, with its polarization vertical to the layers are remarkably reduced, as a result of weakened interlayer coupling in the misfit layer compounds.[27]

Besides the sound velocity, various planar defects in the misfit layer compounds may also reduce the lattice thermal conductivity.[61] As shown in Figure 16, $(PbS)_{1.18}(TiS_2)_2$ shows an ordered structure, where the paired TiS_2 layers and PbS layer are stacked periodically. In contrast, in $(SnS)_{1.2}(TiS_2)_2$ some of the SnS layers show a displacement of b/4 along the b-axis, forming translational disorder. In $(BiS)_{1.2}(TiS_2)_2$, a mixture of staging-1 and staging-2 compounds was found with extensive planar defects. The degree of disordering increases in the order of $(PbS)_{1.18}(TiS_2)_2$, $(SnS)_{1.2}(TiS_2)_2$, and $(BiS)_{1.2}(TiS_2)_2$, which can be confirmed by the increasingly diffused electron diffraction patterns. As shown in Figure 15c, the lattice thermal conductivity also decreases with increasing disorder.

All the misfit layer compounds show relatively high *ZT* values in the in-plane direction (Fig. 15d). However, compared with pure TiS_2, only $(SnS)_{1.2}(TiS_2)_2$ shows a higher *ZT* value. The intercalation of *M*S layer does reduce the lattice thermal conductivity significantly, but the electron transfer effect in $(PbS)_{1.18}(TiS_2)_2$ and $(BiS)_{1.2}(TiS_2)_2$ is too strong, leading to a reduction in the power factor and an increase in the electronic thermal conductivity. It is required to reduce the carrier concentrations of the misfit layer compounds to optimize the thermoelectric performances.

E. Conclusion:

The thermoelectric properties of TiS_2 based materials have been reviewed here. Due to the great flexibility of this structure, lattice part of thermal conductivity can be strongly reduced by inserting cations or block-layer between the CdI_2 type layers or by cationic substitutions. By these different chemical approaches, enhanced *ZT* values up to 0.5 at 700K have been reported, which remains low as compared to best thermoelectric materials. TiS_2 is then seen more as a model structure for the study of the mechanisms which govern the electrical and thermal transport properties, than an efficient thermoelectric material. Nevertheless, the gained knowledge on TiS_2 should serve other layered systems (chalcogenides, oxides) where similar chemical strategies might be applied. In this sense, recent fabrication of hybrid superlattices of alternating inorganic TiS_2 monolayers and organic cations[26] with ultra low thermal conductivity (ZT=0.28 at 373K) is an attractive synthesis route that could lead to the discovery of new high efficiency thermoelectric materials. Transition metal layered lighter chalcogenides might then represent a replacement solution to the long known and used bismuth telluride that seems to suffer from the somewhat erratic price of the tellurium, but also from its relatively high density.

Table 1: The values of the physical parameters are all taken at 700K

	Process conditions		*a* (Å)	*c* (Å)	*ρ* (mΩcm)	*S* (μV/K)	*κ_{total}* (W/mK)	*$\kappa_{lattice}$* (W/mK)	*PF* (mW/mK²)	*ZT*	*n (300K)* ($10^{21}cm^{-3}$)	*μ (300K)* (cm²/Vs)
	Powder synthesis	*SPS*										
TiS_2	1223K/48h+1273K/48h	1073K/10min/50 MPa	3.407(1)	5.704(1)	2.5	-126	1.95	1.27	0.63	0.23	2.7	2.3
$Ti_{0.95}Ta_{0.05}S_2$	"	"	3.404(1)	5.713(1)	1.9	-122	1.92	1.05	0.76	0.28	3.9	2.1
$Ti_{0.9}Ta_{0.1}S_2$	"	"	3.404(1)	5.727(1)	1.1	-94	2.19	0.71	0.75	0.24	4.8	1.7
$Ti_{0.6}Ta_{0.4}S_2$	"	"	3.388(1)	5.781(1)	0.9	-39	2.38	0.55	0.17	0.05	9.3	1.1
TiS_2	905K/12h	873K/30 min/300 MPa	3.405(1)	5.700(1)	28.2	-388	2.39	2.33	0.54	0.16	0.1	10.5
$Ti_{0.99}Nb_{0.01}S_2$	"	"	3.405(1)	5.703(1)	15.1	-317	2.07	1.96	0.66	0.22	0.15	8.5
$Ti_{0.98}Nb_{0.02}S_2$	"	"	3.405(1)	5.703(1)	11.3	-280	2.11	1.96	0.69	0.23	0.29	4.9
$Ti_{0.95}Nb_{0.05}S_2$	"	"	3.404(1)	5.707(1)	7.9	-233	1.97	1.76	0.69	0.24	0.56	3.1
TiS_2	923K/12h	1173K/30min/50 MPa	3.406(1)	5.707(1)	6.9	-264	2.09	1.84	1.01	0.34	0.65	5.6
$Cu_{0.02}TiS_2$	"	"	3.406(1)	5.717(1)	4.2	-217	2.06	1.65	1.12	**0.38**	**1.1**	5.6
$Cu_{0.05}TiS_2$	"	"	3.405(1)	5.733(1)	2.9	-173	1.92	1.32	1.04	**0.38**	**1.91**	4.7
$Cu_{0.1}TiS_2$	"	"	3.407(1)	5.759(1)	1.4	-125	1.99	0.8	1.09	**0.38**	**3.7**	4.5
TiS_2	923K/12h	1073K/30min/50 MPa	3.407(1)	5.700(1)	6.5	-251	2.07	1.81	0.96	0.32		
$Ag_{0.02}TiS_2$	"	"	∅	∅	3.6	-201	1.75	1.25	1.11	**0.44**	∅	∅
$Ag_{0.05}TiS_2$	"	"	∅	∅	2.8	-175	1.75	1.16	1.07	**0.42**	∅	∅
$Ag_{0.1}TiS_2$	"	"	∅	∅	2.1	-154	1.72	0.9	1.12	**0.46**	∅	∅
TiS_2	905K/12	873K/30 min/300 MPa	3.396(1)	5.678(1)	26.8	-388	2.43	2.36	0.56	0.16	0.11	8.6
$Ti_{1.005}S_2$	"	"	3.401(1)	5.684(1)	26.0	-380	2.43	2.36	0.55	0.16	0.13	7.6
$Ti_{1.01}S_2$	"	"	3.405(1)	5.685(1)	31.1	-392	2.35	2.30	0.50	0.15	0.16	4.8
$Ti_{0.015}S_2$	"	"	3.405(1)	5.700(1)	9.4	-293	2.20	2.02	0.91	0.29	0.46	6.9
$Ti_{0.02}S_2$	"	"	3.405(1)	5.700(1)	6.6	-262	1.87	1.61	1.04	**0.39**	**0.52**	7.7
$Ti_{0.025}S_2$	"	"	3.405(1)	5.701(1)	3.4	-192	1.58	1.08	1.08	**0.48**	**1.11**	5.7
$Ti_{0.05}S_2$	"	"	3.414(1)	5.715(1)	0.7	-68	2.83	0.47	0.63	0.16	12.2	1.2
TiS_2	873K/168h	973K/10Min/50MPa	3.396(1)	5.700(1)	1.60	-133	2.41	1.62	1.11	0.24	1.36	6.4
$(PbS)_{1.18}(TiS_2)_2$	1073K/48h	973K/10Min/50MPa	∅	17.451(1)	2.68	-138	1.87	1.16	0.71	0.29	5.30	5.0
$(BiS)_{1.2}(TiS_2)_2$	1073K/48h	973K/10Min/50MPa	∅	16.988(1)	1.01	-90	2.14	0.31	0.81	0.27	2.36	3.1
$(SnS)_{1.2}(TiS_2)_2$	1073K/48h	973K/10Min/50MPa	∅	17.308(1)	2.53	-147	1.71	0.96	0.86	0.39	1.88	5.8

References:

[1] G.S. Nolas, J. Sharp, and H.J. Goldsmid, *Thermoelectric: Basic Principles and New Materials Developments, Springer, New York,* 2001.

[2] T. M. Tritt and M. A. Subramanian, *Thermoelectric Materials, Phenomena and Applications: a Bird's Eye View*, *MRS Bulletin*, 2006, **31.**

[3] H. Imai, Y. Shimakawa, and Y. Kubo, *Phys. Rev. B,* 2001, **64**, 241104.

[4] C. Wan, Y. Wang, N. Wang and K. Koumoto, *Materials*, 2010, **3**, 2606.

[5] E. Guilmeau, Y. Bréard and A. Maignan, *Appl. Phys. Lett*., 2011, **99**, 052107.

[6] M. Beaumale, T. Barbier, Y. Bréard, G. Guelou, A.V. Powell, P. Vaqueiro, and E. Guilmeau, *Acta Materialia*, 2014, **78**, 86.

[7] K. Koumoto, R. Funahashi, E. Guilmeau, Y. Miyazaki, A. Weidenkaff, Y.F. Wang, C.L. Wan, *J. Amer. Ceram. Soc.,* 2013, **96**, 1.

[8] S. Hébert, W. Kobayashi, H. Muguerra, Y. Bréard, R. Nunna, F.Gascoin, E. Guilmeau and A. Maignan, *Phys. Status Sol. A- Applications and Materials Science*, 2013, **210**, 69.

[9] G.A. Wiegers, *Prog. Solid St. Chem.,* 1996, **24**, 1.

[10] L. F. Mattheis, *Phys. Rev. B*, 1973, **8**, 3719.

[11] J. A. Wilson, and A. D. Yoffe, *Advances in Physics,* 1969, **18**, 193.

[12] R. A. Bromley, R. B. Murray, and A. D. Yoffe, *J. Phys. C* 1972, **5**, 759.

[13] P. C. Klipstein, A.G. Bagnall, and W. Y. Liang, *J. Phys. C* 1981, **14**, 4067.

[14] C. M. Fang, R. A. de Groot, and C. Haas, *Phys. Rev. B*, 1997, **56**, 4455.

[15] E. M. Logothetis, W. J. Kaiser, and C. A. Kukkonen, *Physica B*, 1980, **99**, 193.

[16] M. S. Whittingham, and J. A. Panella, *Mat. Res. Bull*., 1981, **16**, 37

[17] A. H. Thompson, F. R. Gamble, and C. R. Symon, *Mat. Res. Bull.* 1975, **10**, 915.

[18] C. A. Kukkonen, O. J. Kaiser, E. M. Logothetis, B. J. Blumenstock, P. A. Schroeder, S. P. Faile, R. Colella, and J. Gambold, *Phys. Rev. B*, 1981, **24**, 1691.

[19] H. Kobayashi, K. Sakashita, M. Sato, T. Nozue, T. Suzuki, and T. Kamimura, *Physica B*, 1997, **237**, 169

[20] M. J. McKelvy, and W. S. Glaunsinger, *J. Solid State Chem*., 1987, **66**, 181.

[21] A. Amara, Y. Frongillo, M. J. Aubin, S. Jandl, J. M. Lopez-Castillo, and J. P. Jay-Gerin, *Phys. Rev B*, 1987, **36**, 6415

[22] Meerschaut, A.; Auriel, and C.; Rouxel, *J. Alloy Compd.,* 1992, **183**, 129.

[23] T. Barbier, O. I. Lebedev, V. Roddatis, Y. Bréard, A. Maignan, and E. Guilmeau, *Dalton Transactions*, 2015, DOI: 10.1039/C5DT00551E

[24] M. Beaumale, T. Barbier, Y. Bréard, S. Hébert, Y. Kinemuchi, and E. Guilmeau, *J. Appl. Phys*. 2014, **115**, 043704

[25] M. Beaumale, T. Barbier, Y. Bréard, B. Raveau, Y. Kinemuchi, R. Funahashi, and E. Guilmeau, *J. Elec. Mater*. 2014, **43**, 1590

[26] C.L. Wan, K.K. Gu, F. Dang, T. Ito, Y.F. Wang, H. Sasaki, M. Kondo, K. Koga, K. Yabuki, G.J. Snyder, R.G. Yang, and K. Koumoto, *Nat. Mater*. 2015, DOI: 10.1038/NMAT4251

[27] C.L. Wan, Y.F. Wang, N. Wang, W. Norimatsu, M. Kusunoki, and K. Koumoto, *J. Elec. Mater*., 2011, **40**, 1271.

[28] C. Wan, Y. Wang, N. Wang, W. Norimatsu, M. Kusunoki and K. Koumoto, *Sci. Technol. Adv. Mater.* 2010, **11**, 044306.

[29] M. Inoue, H.P. Hughes and A.D. Yoffe, *Adv. Phys*. 1989, **38**, 565.

[30] J.I. Meakin, and P.C. Klipstein, *J. Phys. C: Solid State Phys*. 1987, **20**, 271.

[31] A. Saxena and J.D. Gunton, *Acta Cryst*. 1986, **A42**, 399.

[32] G. A. Scholz, and R. F. Frindt, *Mater. Res. Bull*. 1980, **15**, 1703.

[33] K.K. Bardhan, G. Kirczenow, G. Jackle and J.C. Irwin, *Phys. Rev. B*, 1986, **33**, 4149.

[34] D. Li, X.Y. Qin, J. Liu, and H.S. Yang, *Phys. Lett. A* 2004, **328**, 493.

[35] B.G. Silbernagel, and M.S. Whittingham, *Mater. Res. Bull*. 1976, **11**, 29.

[36] P.C. Klipstein and R.H. Friend, *J. Phys. C: Solid State Phys*. 1987, **20**, 4169.

[37] T. Kawasaki and K. Ohshima, *J. of the Phys. Soc. Jpn* 2011, **80**, 044601.

[38] P.M. Danot and R. Brec, *Acta Cryst. B*, 1975, **31**, 1647.

[39] G.A. Wiegers, K.D. Bronsema, S. Van Smaalen, R.J. Haange, J.E. Zondag and J.L. De Boer, *J. Solid State Chem*., 1987, **67**, 9.

[40] Y. Jeannin, and J. Benard, *Compt Rend* 1959, **248**, 2875.

[41] Y. Jeannin, *Compt Rend* 1960, **251**, 246.

[42] J.C. Mikkelsen, *Nuevo Cimento*, 1977, **38**, 378

[43] M. Ohta, S. Satoh, T. Kuzuya, S. Hirai, M. Kunii, and A. Yamamoto, *Acta Materialia*, 2012, **60**, 7232

[44] F. Gascoin, R. Nunna, E. Guilmeau, and Y. Bréard, *J. All. Comp.* 2012, **521**, 121.

[45] D. Li, X.Y. Qin, J. Zhang, and H.J. Li. *Phys Lett A*, 2006, **348**, 379.

[46] D. Li, X.Y. Qin, J. Liu, and H.S. Yang, *Phys Lett A*, 2004, **328**, 493

[47] E.E. Abbott, J.W. Kolis, N.D. Lowhorn, W. Sams, A. Rao, T.M. Tritt, *Appl. Phys. Lett.,* 2006, **88**, 262106

[48] A.F. Ioffe, S.V. Airepetyants, A.V. Ioffe, N.V. Kolomoets, and L.S. Stil'bans, *Dokl. Akad. Nauk. SSSR*, 1956, **106**, 981.

[49] T. M. Tritt, 2000a *Semiconductors and Semimetals, Recent Trends in Thermoelectric Materials Research*, Academic Press, San Diego, **Vol. 69–71**

[50] A.H. Thompson, K.R. Pisharody, and R.F. Koehler, *Physical Review Letters*, 1972, **29**, 163.

[51] J.A. Benda, *Physical Review B*, 1974, **10**, 1409.

[52] F.J. Di Salvo, J.A. Wilson, B.G. Bagley and J.V. Waszczak, *Physical Review B*, 1975, **12**, 2220.

[53] Y. Tison, H. Martinez, I. Baraille, M. Loudet, and D. Gonbeau, *Surface Science*, 2004, **563**, 83.

[54] M. Shimakawa, H. Maki, H. Nishihara, and K. Hayashi, *Mater. Res. Bull*., 1997, **32**, 689.

[55] L.E. Conroy, and K.R. Pisharody, *Solid State Chemistry : Proceeding of the 5th materials Research Symposium, National Bureau of Standards, Special publication*, 1972, **364**.

[56] J. M. Tarascon, F. J. DiSalvo, M. Eibschutz, D. W. Murphy, and J. V. Waszczak, *Phys Rev B*, 1983, **28**, 6397.

[57] H. P. Vaterlaus, F. Lévy, and H. Berger, *J. Phys. C:Solid State Physics*, 1983, **16**, 1517

[58] D.T. Hodul, *J. Solid State Chem*. 1986, **62**, 328

[59] S.K. Srivastava, T.K. Mandal, and B.K. Samantaray, *Synth. Met*. 1997, **90**, 135.

[60] J. Callaway, *Phys. Rev*., 1959, **113**, 1046.

[61] C. Wan, Y. Wang, W. Norimatsu, M. Kusunoki, and K. Koumoto, *Appl. Phys. Lett*. 2012, **100**, 101913

Figure captions:

Figure 1: Schematic representations of a) TiS_2, b) $(Ag,Cu)_xTiS_2$, stage 1 and c) $Ag_{0.167}TiS_2$, stage 2.

Figure 2: Crystal structure of $(PbS)_{1.18}(TiS_2)_2$ along the incommensurate direction

Figure 3: Evolution of the c cell-unit parameter in Cu_xTiS_2 and Ag_xTiS_2 series

Figure 4: ED patterns of a) $Ag_{0.05}TiS_2$ and b) $Ag_{0.2}TiS_2$ taken along [010] zone axis, c) [010] HRTEM image of $Ag_{0.1}TiS_2$ sample. Local incorporation of stage 2 structure in form of defects is marked with white arrows. The [010] ED pattern is given as an inset.

Figure 5: Electrical resistivity and Seebeck coefficient (700K) as a function of x in Cu_xTiS_2 and Ag_xTiS_2 series.

Figure 6: Thermal conductivity and its lattice component as a function of x in Cu_xTiS_2 and Ag_xTiS_2 series.

Figure 7: Temperature dependence of the electrical resistivity in the $Ti_{1+x}S_2$ series

Figure 8: Seebeck coefficient as a function of x in $Ti_{1+x}S_2$ at 300 K of our study, along with those previsously reported.

Figure 9: Thermal conductivity and its lattice component as a function of x in $Ti_{1+x}S_2$ series.

Figure 10: [010] HRTEM image of $Ti_{0.025}S_2$ sample. Local intercalation of Ti forming "wavy" defects are marked with white arrows.

Figure 11: [110] HRTEM image of $Ti_{0.9}Ta_{0.1}S_2$ sample.

Figure 12: Temperature dependence of a) electrical resistivity and b) Seebeck coefficient in the $Ti_{1-x}Ta_xS_2$ and $Ti_{1-x}Nb_xS_2$ series.

Figure 13: Temperature dependence of the thermal conductivity and its lattice component (κ_L) in the series $Ti_{1-x}Ta_xS_2$.

Figure 14: Temperature dependence of the thermal conductivity and its lattice component (κ_L) in the series $Ti_{1-x}Nb_xS_2$.

Figure 15 Seebeck coefficients (a), electrical conductivities (b),lattice thermal conductivities (c), and ZT values (d) of TiS_2 and $(MS)_{1+x}(TiS_2)_2$.

Figure 16: TEM images and electron diffraction patterns (left), simulated crystal structure (right) of $(PbS)_{1.18}(TiS_2)_2$ (a), $(SnS)_{1.2}(TiS_2)_2$ (b) and $(BiS)_{1.2}(TiS_2)_2$ (c) along the [100] zone axis.

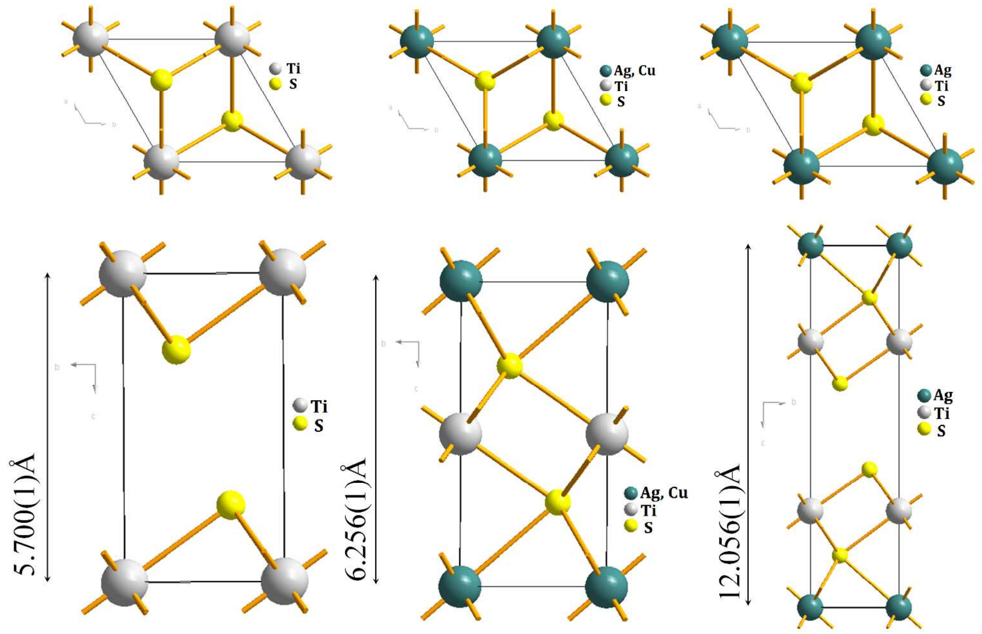

a) TiS_2

b) $(Ag, Cu)_xTiS_2$ Stage 1

c) $Ag_{0.167}TiS_2$ Stage 2

Figure 1

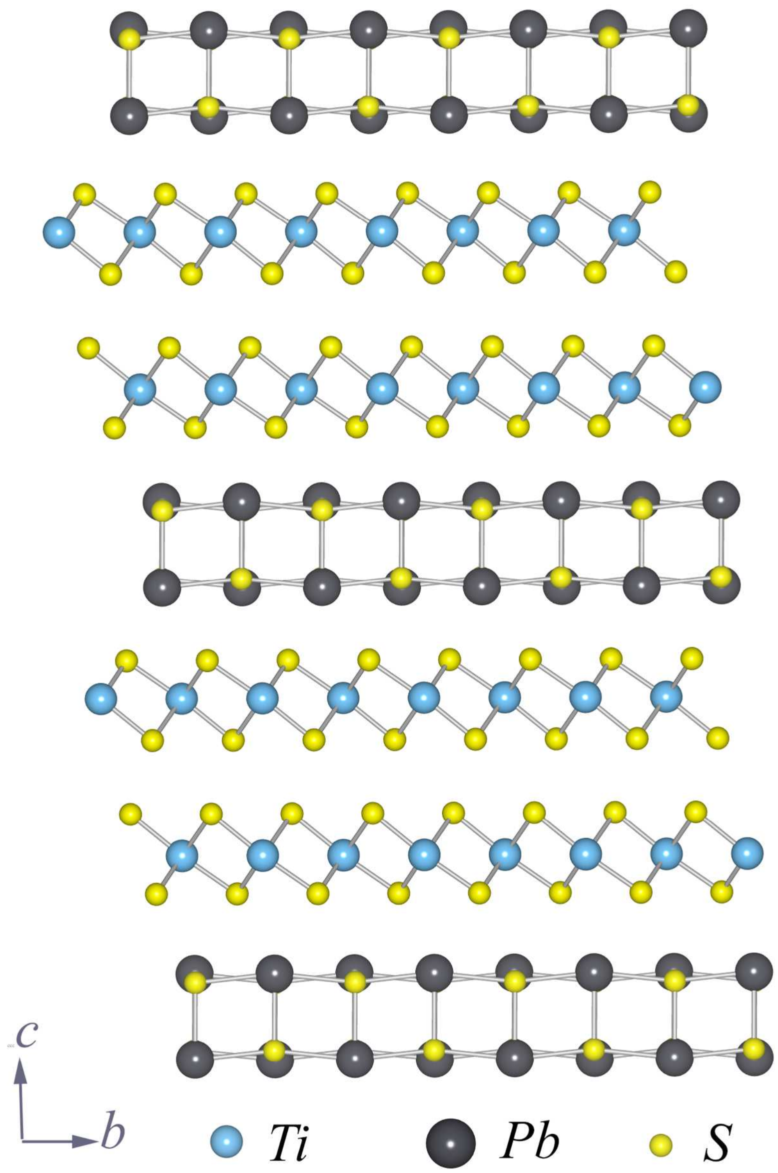

Figure 2
560x776mm (72 x 72 DPI)

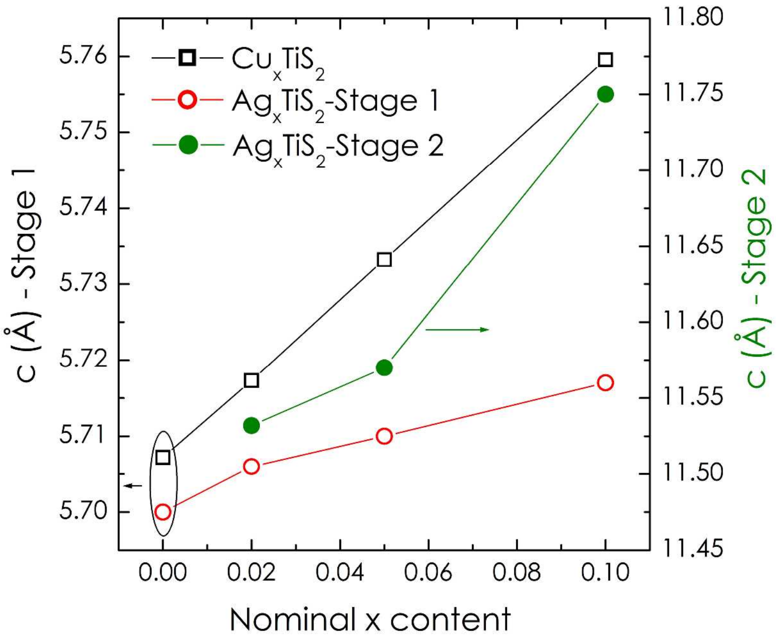

Figure 3
1147x806mm (150 x 150 DPI)

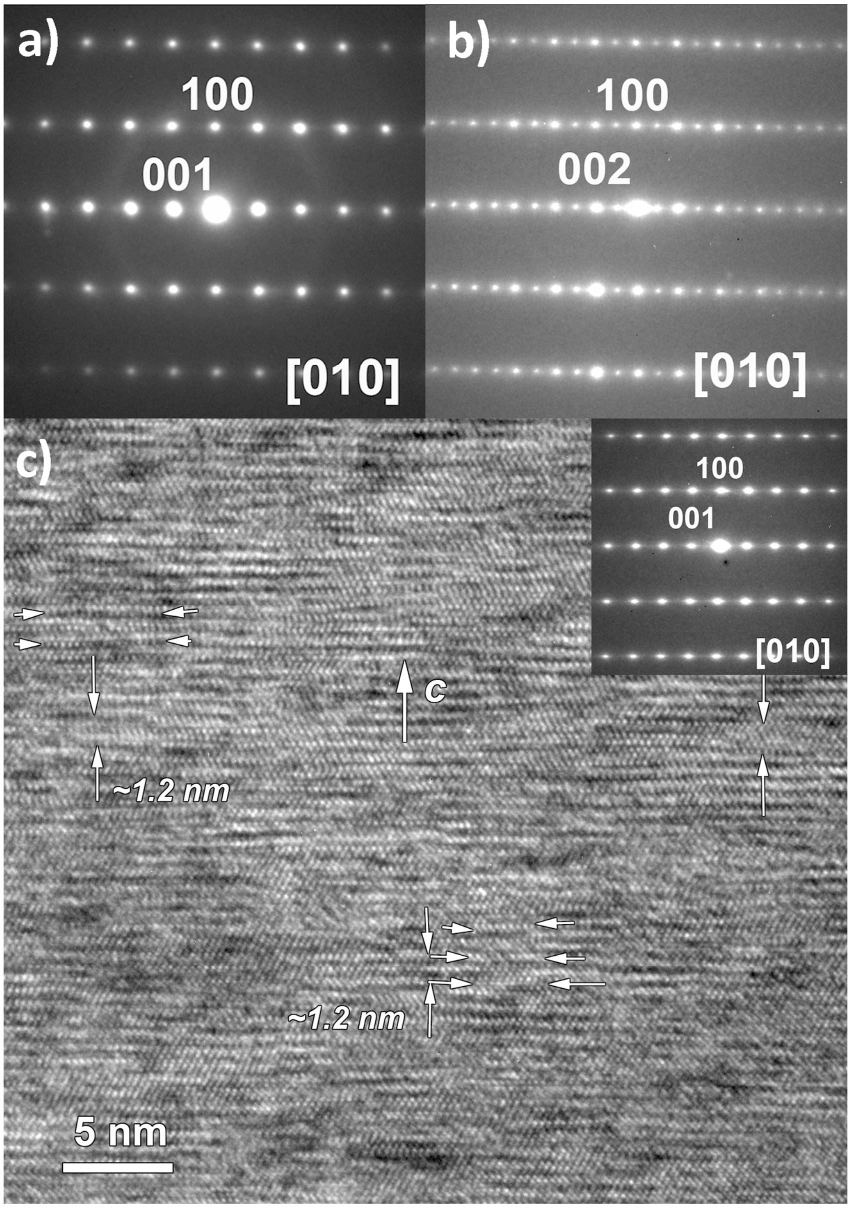

Figure 4
132x188mm (300 x 300 DPI)

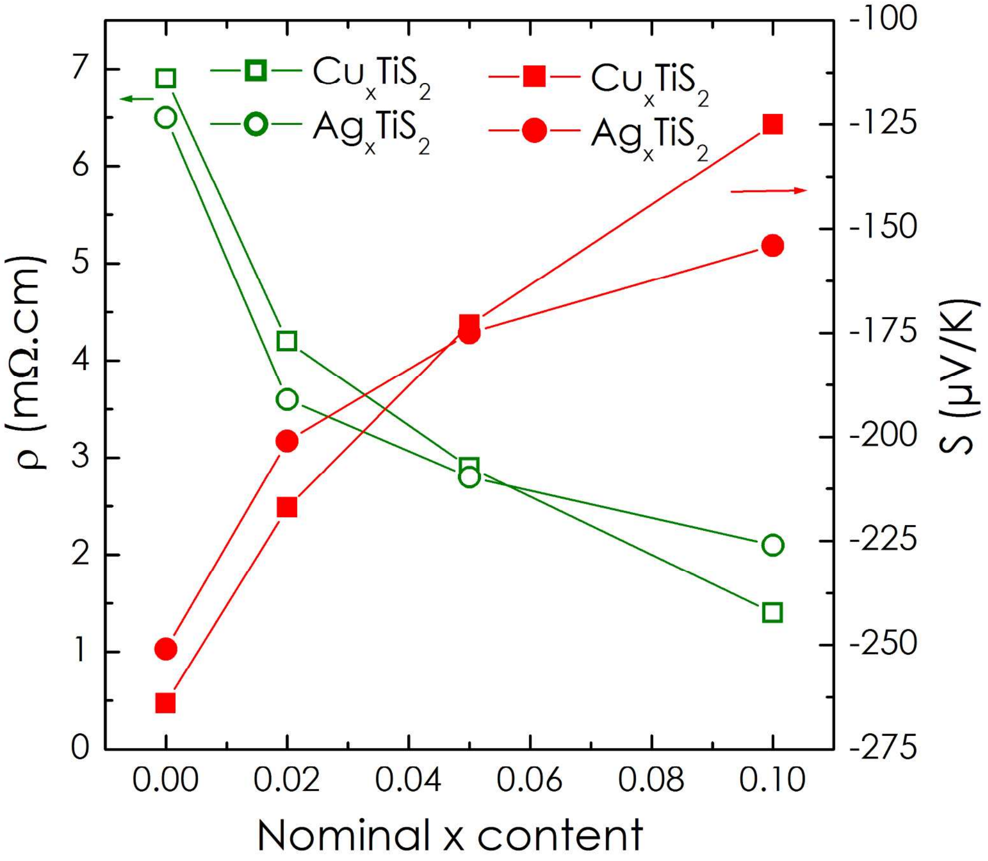

Figure 5
418x367mm (150 x 150 DPI)

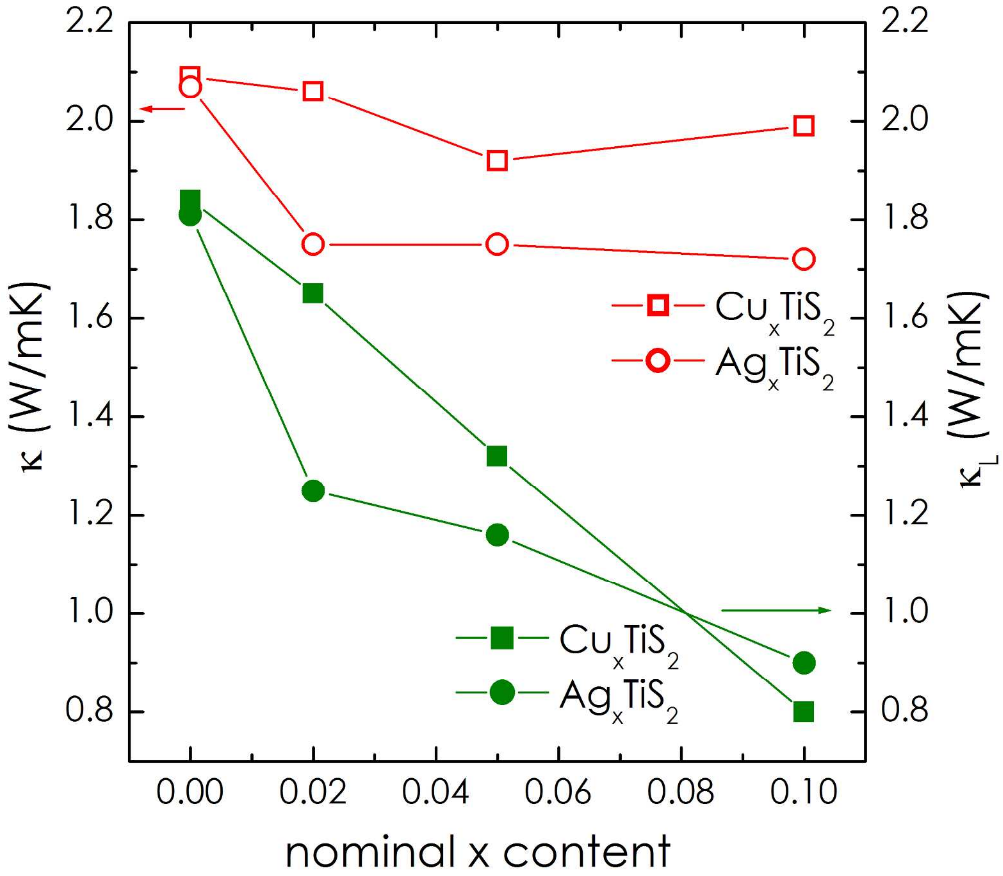

Figure 6
413x360mm (150 x 150 DPI)

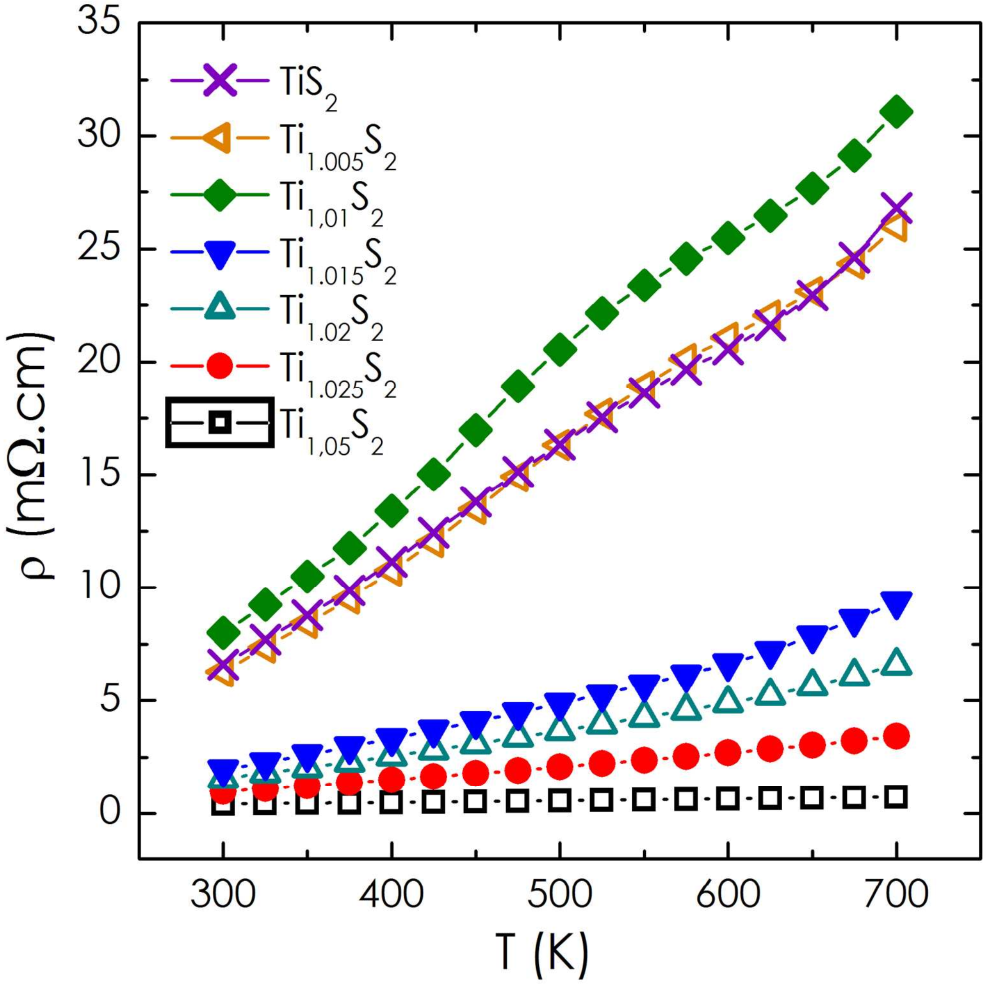

Figure 7
360x358mm (150 x 150 DPI)

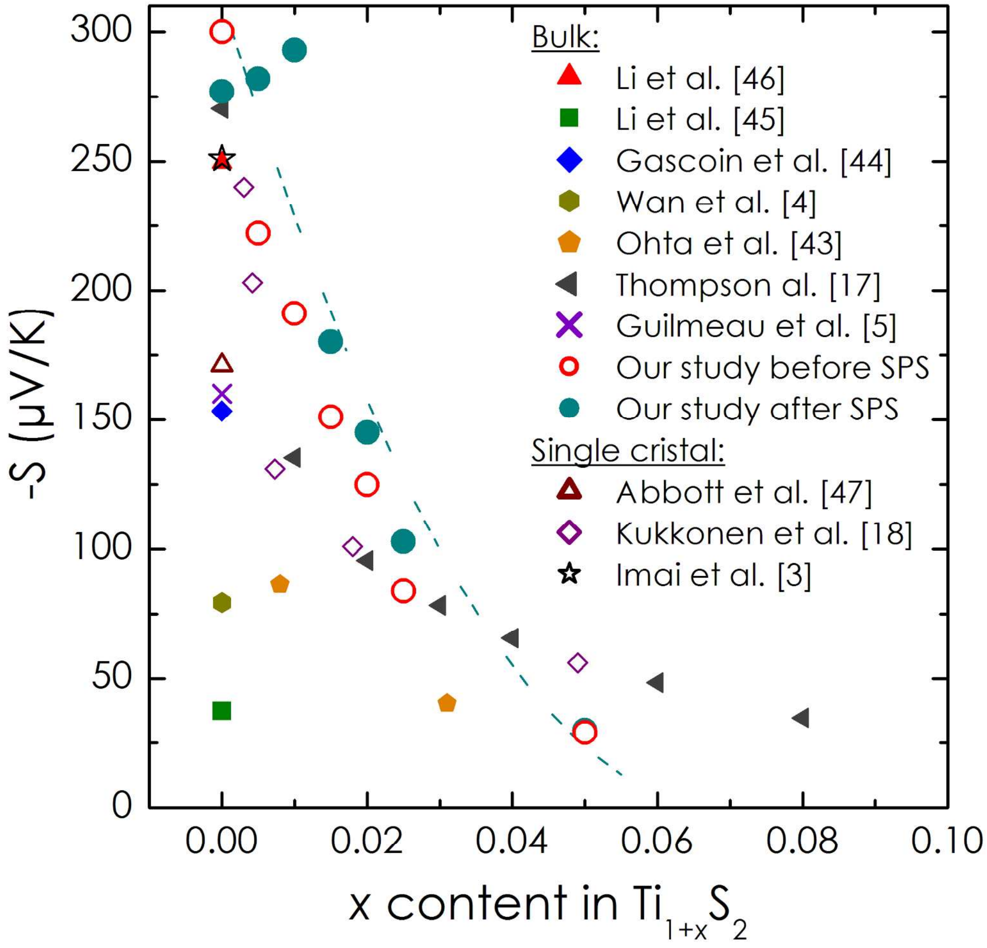

Figure 8
384x367mm (150 x 150 DPI)

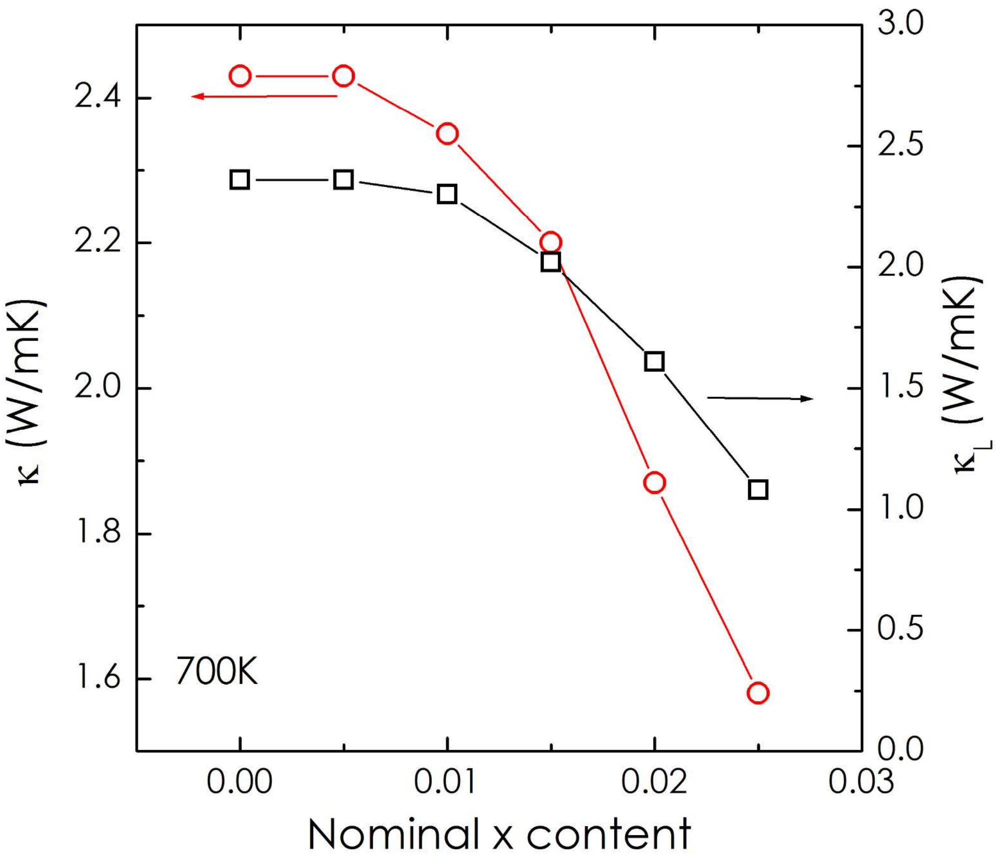

Figure 9
420x359mm (150 x 150 DPI)

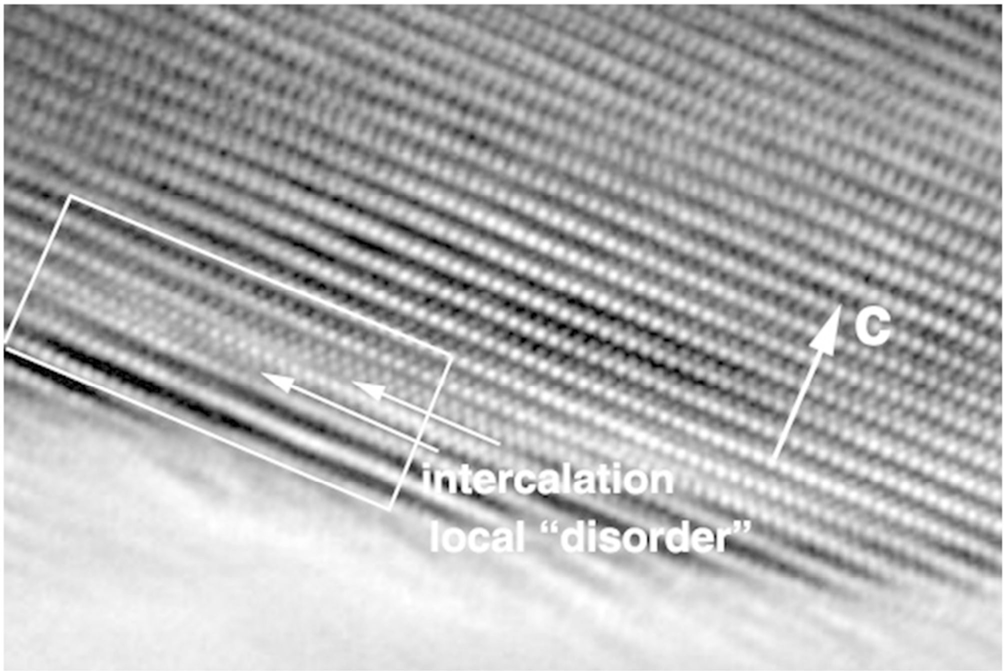

Figure 10
74x49mm (300 x 300 DPI)

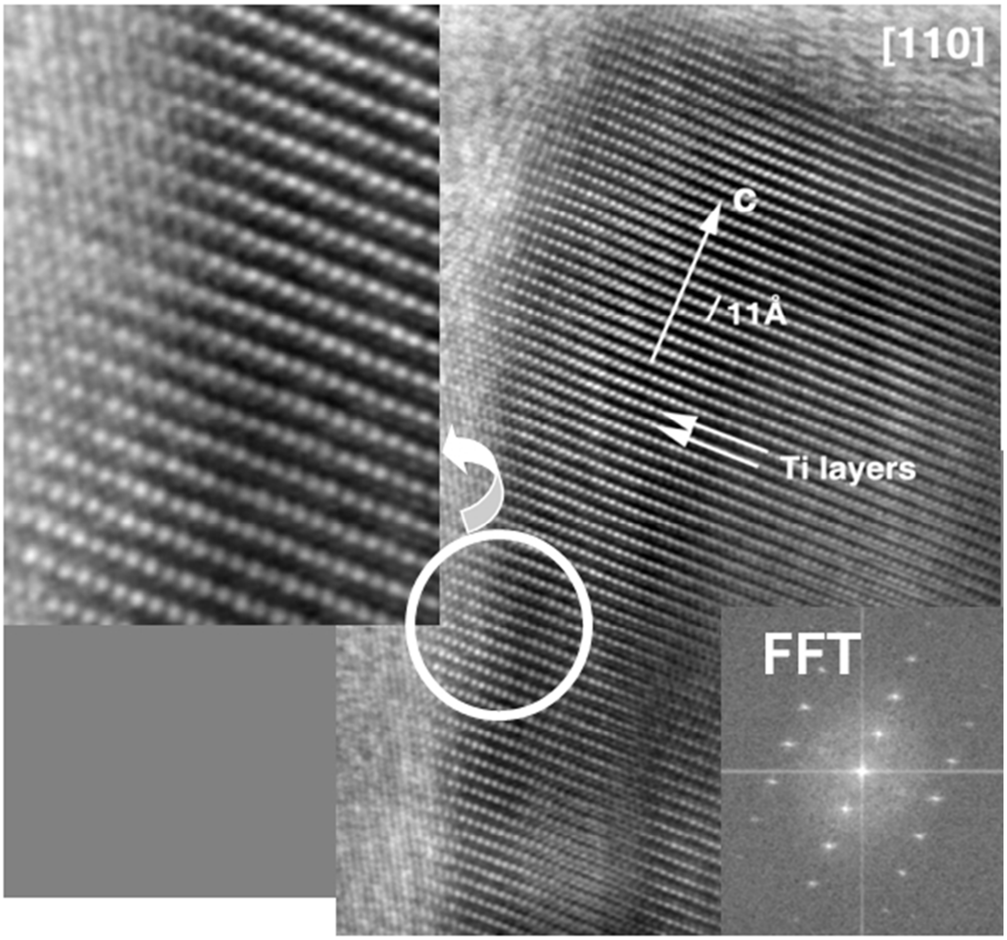

Figure 11

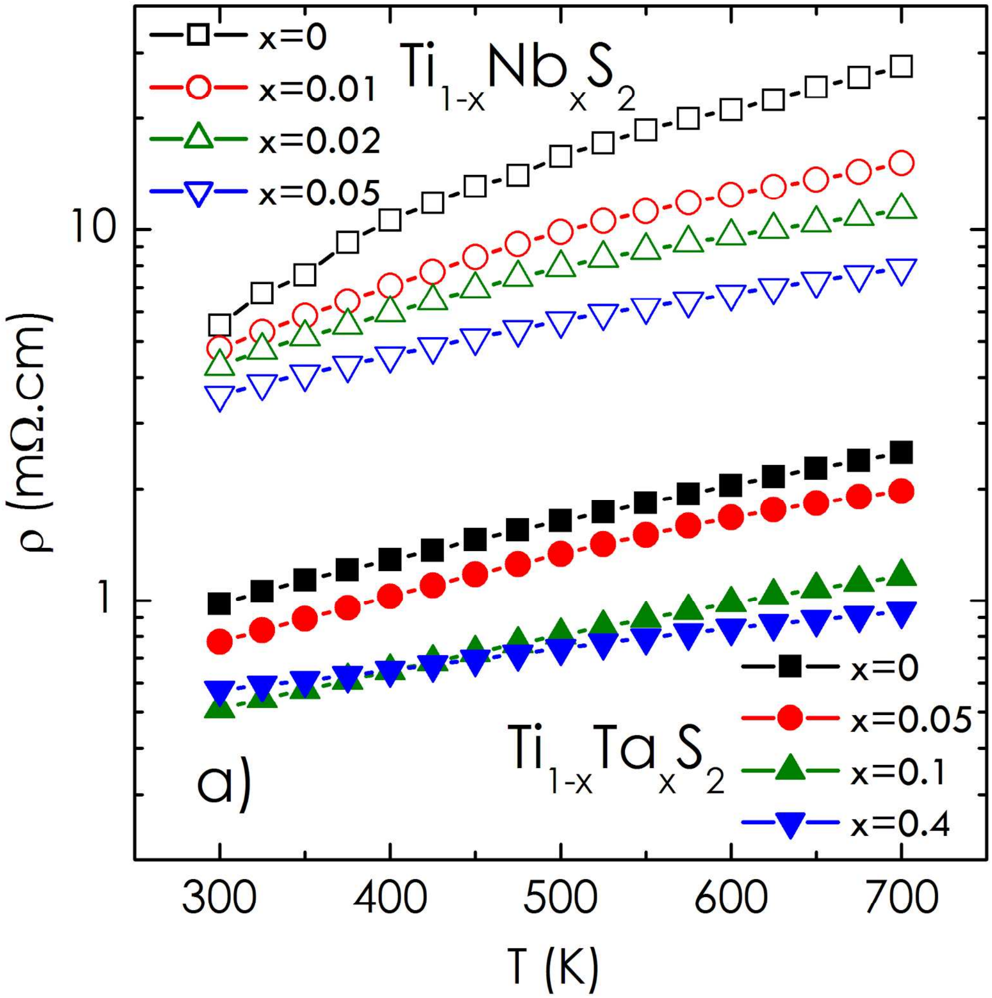

Figure 12a
367x369mm (150 x 150 DPI)

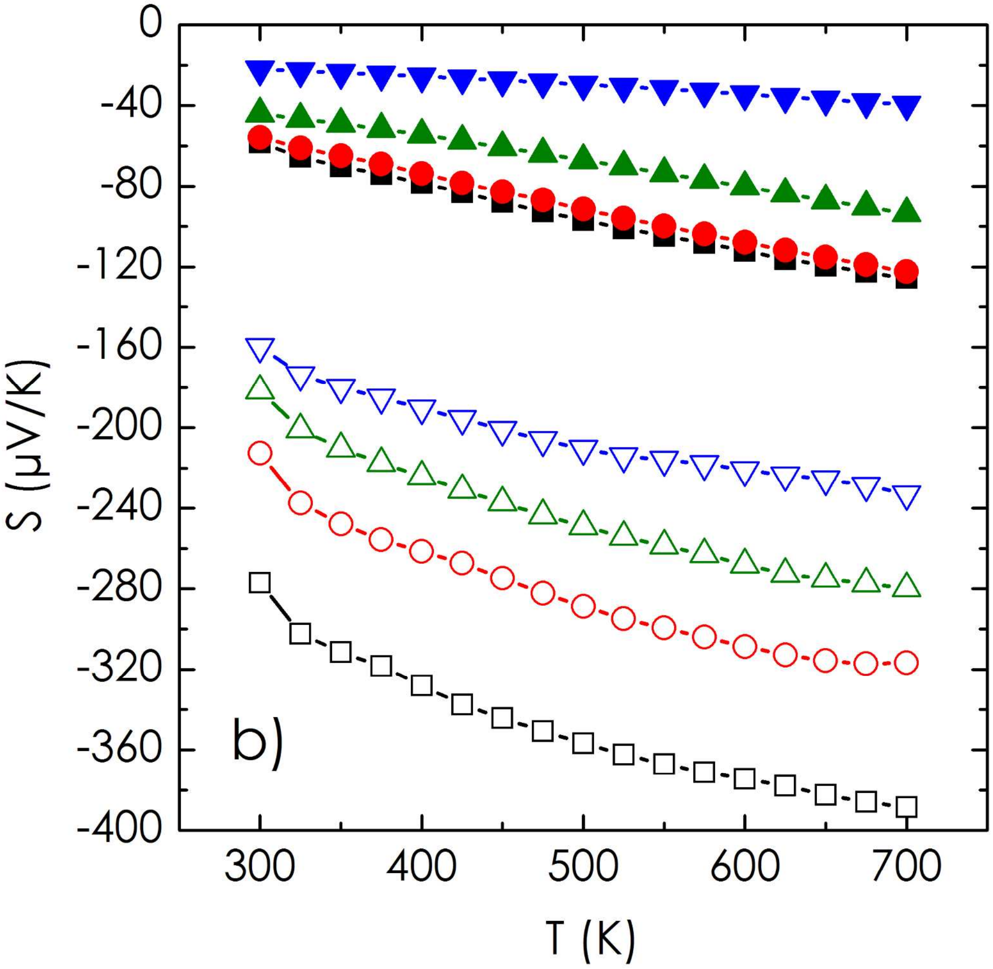

Figure 12b
389x378mm (150 x 150 DPI)

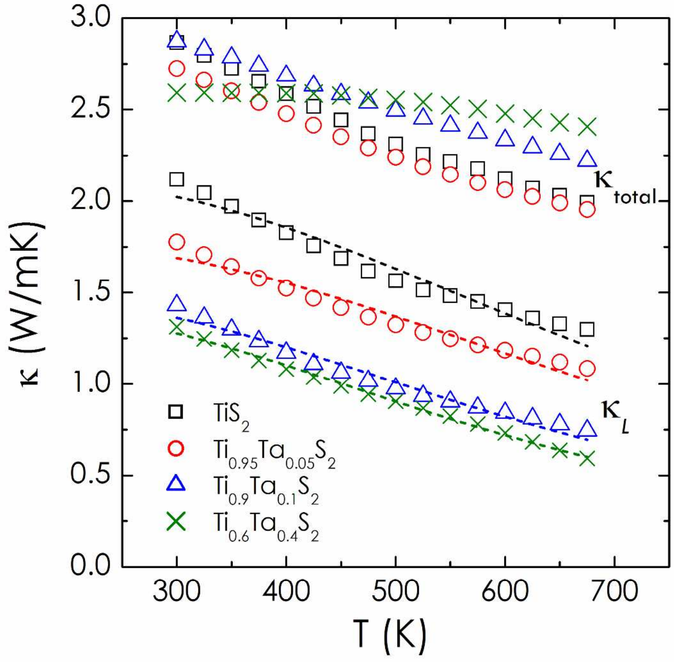

Figure 13
573x403mm (150 x 150 DPI)

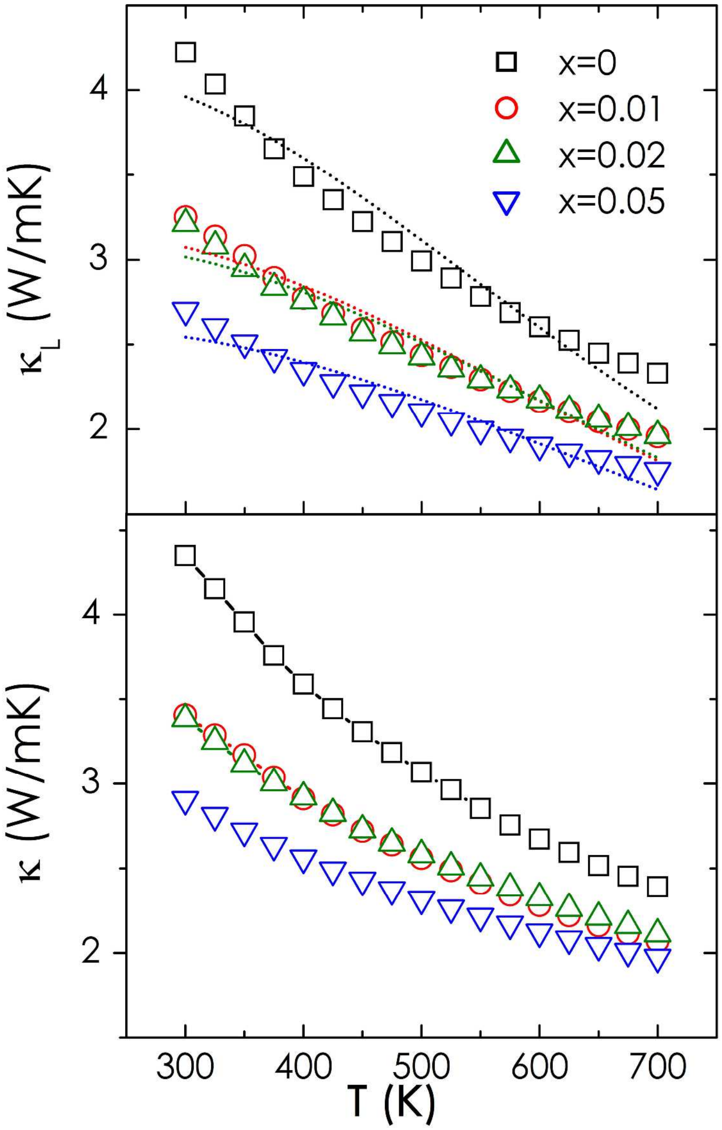

Figure 14
806x1147mm (150 x 150 DPI)

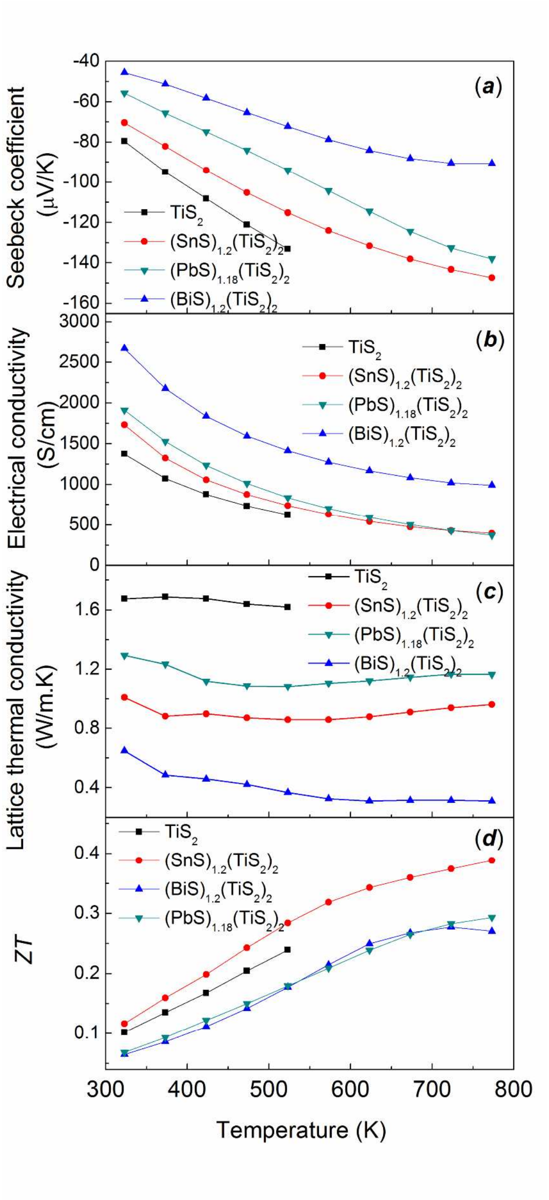

Figure 15
186x410mm (300 x 300 DPI)

(a) $(PbS)_{1.18}(TiS_2)_2$

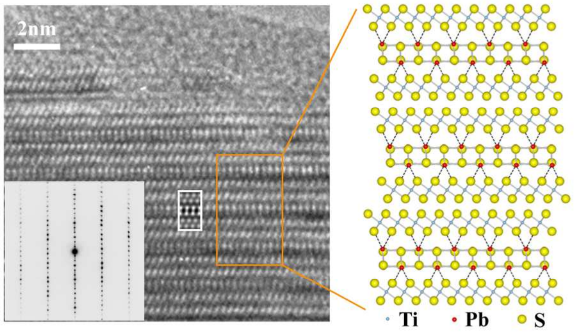

(b) $(SnS)_{1.2}(TiS_2)_2$

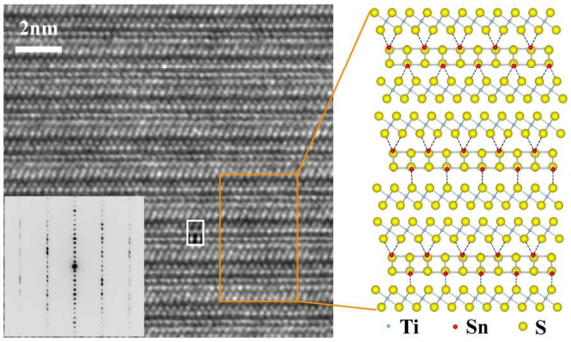

(c) $(BiS)_{1.2}(TiS_2)_2$

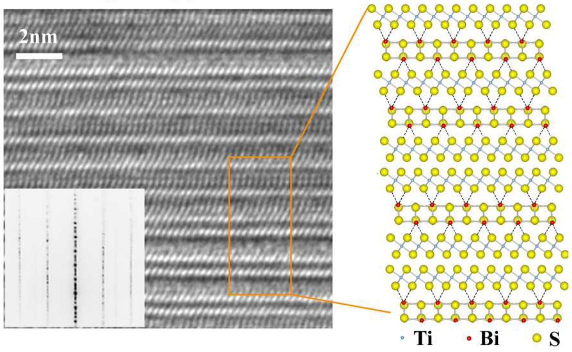

Figure 16
209x424mm (150 x 150 DPI)